Synthesis and Characterization of a Dinuclear Manganese(III,III) Complex with Three Phenolate Ligands

Reiner Lomoth,[a] Ping Huang,[b] Jiutian Zheng,[c] Licheng Sun,*[c] Leif Hammarström,*[a] Björn Åkermark,[c] and Stenbjörn Styring*[b]

Keywords: Manganese / Ligand design / Redox chemistry

A dinuclear manganese complex ($[Mn_2L(\mu\text{-}OAc)_2]PF_6$) has been synthesized, where L is the trianion of 2,6-bis{[(2-hydroxy-3,5-di-*tert*-butylbenzyl)(2-pyridylmethyl)amino]-methyl}-4-methylphenol, a ligand with three phenolate groups. The two pseudo-octahedrally coordinated Mn ions are bridged via the two bidentate acetate ligands and the 4-methylphenolate group of the ligand. We have characterized the complex with electrochemistry, spectroelectrochemistry and EPR spectroscopy. Electrochemically the $Mn_2^{III,III}$ complex undergoes two metal-centered quasi-reversible one-electron reduction steps ($E_{1/2}$ = 0.04 and −0.32 V vs. SCE). Reduction to the $Mn_2^{II,III}$ state results in transformation into a modified complex with slightly different redox properties. One-electron oxidation ($E_{1/2}$ = 0.96 V vs. SCE) affords the $Mn_2^{III,IV}$ state while further one-electron oxidation ($E_{1/2}$ = 1.13 V vs. SCE) presumably involves ligand oxidation. High valent Mn complexes involving Mn^{IV} or Mn^{V} centers are of particular interest as intermediates in catalytic water oxidation. The redox potentials of $[Mn_2L(\mu\text{-}OAc)_2]^+$ show the expected stabilization of higher manganese oxidation states compared with the related complex, $[Mn_2(bpmp)(\mu\text{-}OAc)_2]^+$.

Introduction

A major reason for the interest in higher valent multinuclear manganese complexes is the catalytic activity of the $(Mn)_4$ cluster in photosynthetic water oxidation.[1] This is a key reaction in nature that provides the electrons needed for the reduction of CO_2 resulting in energy rich reduced carbon products. Therefore, synthetic Mn complexes have potential importance for the construction of artificial photosynthetic systems to convert solar energy into fuels.[2] The oxygen evolving center (OEC) in photosynthesis, as well as artificial systems aiming for fuel production by light-induced water splitting, has to involve a catalyst that can store four oxidation equivalents generated by subsequent light-induced one-electron oxidations. Finally the catalyst has to retrieve all four electrons from water since oxidation of water can be accomplished at a reasonable potential (0.82 V vs. NHE at pH 7) only in a four-electron process. In photosynthesis catalytic water oxidation is carried out in Photosystem II by the OEC, an oxo-bridged tetranuclear manganese complex that cycles between five redox states.[1]

In our attempts to mimic the electron transfer reactions on the electron donor side of Photosystem II we have, earlier, studied the light-induced oxidation of manganese complexes sensitized by $[Ru(bpy)_3]^{2+}$ (bpy = 2,2′-bipyridine) and we recently observed the light-induced three-step oxidation of the $Mn_2^{II,II}$ dimer $[Mn_2(bpmp)(\mu\text{-}OAc)_2]^+$ [3] to a $Mn_2^{III,IV}$ dimer in an aqueous/acetonitrile medium.[4]

Although the exact mechanism of photosynthetic water oxidation is not solved, it is clear that some of the steps in the cyclic redox reactions (the so called S-cycle) involve Mn-centered oxidations.[5] It is also clear that the Mn ions in the higher oxidation states of the S-cycle are at the Mn^{III} state or higher. A $Mn^{V}{=}O$ moiety has been proposed to play a key-role in O−O bond formation in both photosynthesis[6] as well as in a model complex.[7] With regard to the importance of high-valent manganese species for catalytic water oxidation, we have commenced with the synthesis of manganese complexes with an increased number of negatively charged ligand functions to stabilize higher oxidation states of manganese. In this paper we on report the synthesis and characterization of complex **4**, which is the $Mn_2^{III,III}$ dimer $[Mn_2L(\mu\text{-}OAc)_2]^+$, where L is the trianion of 2,6-bis{[(2-hydroxy-3,5-di-*tert*-butylbenzyl)(2-pyridylmethyl)amino]methyl}-4-methylphenol. The complex con-

[a] Department of Physical Chemistry, Uppsala University, P. O. Box 532, 751 21 Uppsala, Sweden
Fax: (internat.) + 46-18/508542
E-mail: Leifh@fki.uu.se
[b] Department of Biochemistry, Center for Chemistry and Chemical Engineering, Lund University, P. O. Box 124, 221 00 Lund, Sweden
Fax: (internat.) + 46-46/2224534
E-mail: stenbjorn.styring@biokem.lu.se
[c] Department of Organic Chemistry, Arrhenius Laboratories, Stockholm University, 106 91 Stockholm, Sweden
Fax: (internat.) + 46-8154908
E-mail: licheng.sun@organ.su.se
Supporting information for this article is available on the WWW under http://www.eurjic.org or from the author.

tains a bridging phenolate and two additional phenolate groups that replace two of the pyridyl groups in the $[Mn_2(bpmp)(\mu\text{-}OAc)_2]^+$ complex resulting in considerably lowered redox potentials for the manganese redox couples. Thus, the high valent Mn states that are of interest for water oxidation may also be accessible with photochemical oxidation, using photo-oxidants such as $[Ru(bpy)_3]^{2+}$.

Results and Discussion

Synthesis

A ligand similar to the one used here has been employed for the preparation of $Fe_2^{II,III}$ and $Fe_2^{III,III}$ complexes[8] but no Mn dimer with this type of $(N_2O_2)_2$-μ-O compartmental ligand has been prepared. We have introduced *tert*-butyl substituents on the phenol groups of the ligand to increase their electron donating effect and to improve the solubility of the complex. Apart from that the *tert*-butyl groups seem to ease the isolation of the Mn complex since we were not able to isolate the analogue Mn complexes with unsubstituted or methyl-substituted phenol groups.

The synthesis of the ligand precursors is shown in Scheme 1. The Schiff base intermediate was made by a condensation reaction of 3,5-di-*tert*-butyl-2-hydroxybenzaldehyde and picolylamine. The reduction of the Schiff base by sodium hydroborate gave the secondary amine **1**. 2,6-dichloromethyl-4-methylphenol **2** was synthesized by reaction of 2,6-dihydroxy-4-methylphenol, which was prepared by the procedure shown in Scheme 1 (see b).

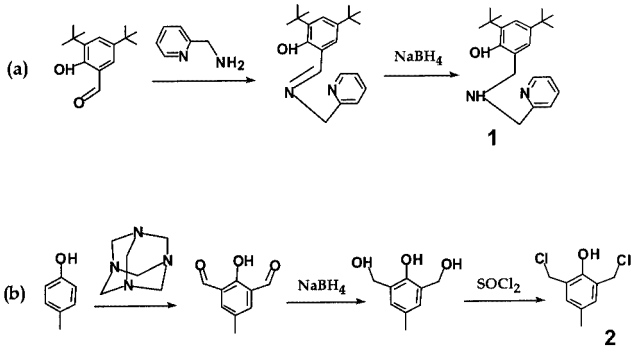

Scheme 1

Two different routes have been used to synthesize the ligand **3** in reasonable yields (Scheme 2). In route A, the secondary amine **1** was reacted directly with *p*-cresol and paraformaldehyde in a modified Mannich reaction in an ethanol/water mixture. Alternatively, **3** was obtained from the reaction of the secondary amine **1** and 2,6-dichloromethyl-4-methylphenol **2** according to route B.

Reaction of manganese(III) acetate in ethanol with **3** gave the manganese(III,III) dimer complex $[Mn_2L(\mu\text{-}OAc)_2]^+$, **4**, where L is the trianion of **3**. Elemental analysis, ESI-MS (see Exp. Sect.), electrochemistry, spectroelectrochemistry, and EPR spectroscopy (see below) were used to characterize the complex. In ESI-MS spectra the base peak was attributed to the mono-charged $Mn_2^{III,III}$ dimer complex.

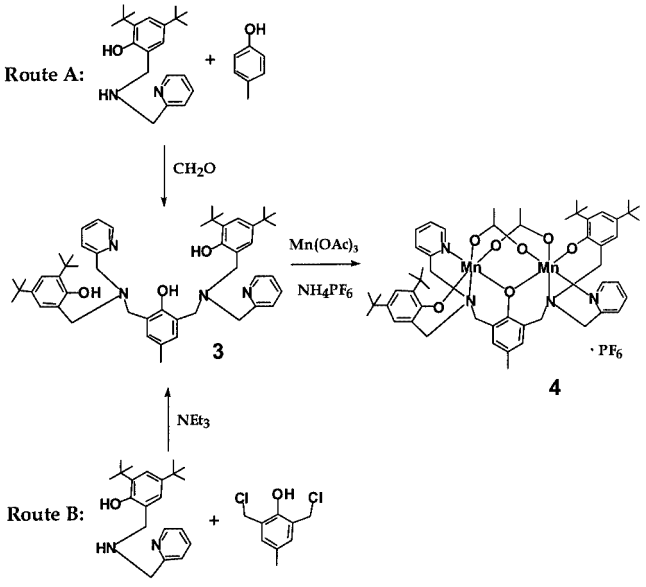

Scheme 2

In addition to the base peak a minor peak at a higher *m*/*z* region was observed that can be assigned to a trace of a $Mn_4^{III,III,III,III}$ tetramer $[\{Mn_2L(\mu\text{-}OAc)_2\}_2(PF_6)]^+$ with one counterion. The tetramer has exactly twice the mass of the dimer, suggesting either a weak association between two structurally intact dimers, or a true tetramer with acetates crossbridging between the dimer units. The tetramer could be formed during the ionization process in ESI-MS, but the fact that these tetramers may have been formed during the synthesis cannot be excluded.

Complex **4** can be expected to exist in two diastereomeric forms with the pyridine nitrogens *syn* or *anti* to the Mn−O(phenolate)−Mn plane. Within the limits of spectral resolution no indication for a mixture of different diastereomers in the preparation of **4** was obtained by any of the spectroscopic methods applied.

Several attempts to crystallize **4** failed.

Spectroscopic and Electrochemical Characterization of 4

We will begin by describing the spectroscopic and electrochemical characterization of **4**. In the following sections we will then describe the characterization of the different products obtained by reduction or oxidation of **4**.

Magnetic Susceptibility Measurements

The molar magnetic susceptibility χ in a powder sample of **4**(PF_6) was measured as a function of temperature between 2 and 300 K. The product χT amounts to 5.34 $cm^3mol^{-1}K$ at 300 K and decreases to 0.21 $cm^3mol^{-1}K$ at 2 K (not shown). The temperature behavior reveals antiferromagnetic coupling between the Mn^{III} sites and the high value of χT at 300 K indicates a weak coupling interaction. The best fit of the data was obtained with a *g*-factor of 1.99

and a fraction of dimer of $F = 0.961$ and resulted in an exchange coupling constant of $J = -8.5$ cm^{-1}. Weak antiferromagnetic coupling with similar values of $-J = 5-8$ cm^{-1} has been reported for other $Mn_2^{II,III}$ and $Mn_2^{II,II}$ complexes with a (μ-phenoxo)bis(μ-acetato) core.[9] No reference data is available for $Mn_2^{III,III}$ complexes with the same bridging structure but the difference between the $Mn_2^{II,III}$ and $Mn_2^{II,II}$ states of $[Mn_2(bpmp)(\mu\text{-}RCOO)_2]^{+/2+}$ [10] is small and similar behavior might be expected for the $Mn_2^{III,III}$ complex **4**, supporting its (μ-phenoxo)bis(μ-acetato) formulation.

EPR Spectroscopy

The perpendicular mode EPR spectrum of **4** is shown in Figure 1 (see c). This spectrum is essentially silent as expected for a $Mn_2^{III,III}$ dimer with an integral spin. Moreover, no signals were detected with parallel mode EPR (not shown). The absence of a parallel mode signal has been interpreted as an indication for antiferromagnetic coupling between two Mn^{III} ions, resulting in an $S = 0$ singlet ground spin state.[11] Magnetic susceptibility measurements of **4** clearly reveal weak antiferromagnetic coupling between the two Mn^{III} ions (see above). Weak multiline signals centered at $g \approx 2$ in the perpendicular mode spectrum (see c in Figure 1) can be assigned to traces of a $Mn_2^{II,III}$ species (ca. 4100−4600 G) and a $Mn_2^{III,IV}$ species (ca. 2900−4000 G) that amount to $< 5\%$ and $< 1\%$ of the total Mn, respectively (for details of the quantification see Exp. Sect.). Thus, the dominating part ($> 94\%$) of the material is an EPR silent $Mn_2^{III,III}$ dimer, as expected. The $Mn_2^{II,III}$ signal probably arises from the reduced state of **4**.

UV/Vis Spectroscopy

Figure 2 shows the electronic spectrum of **4** and its oxidation and reduction products in acetonitrile. On the basis of similarities with the spectra of other Mn complexes and the spectral changes observed upon oxidation and reduction (see below), the following assignments of the electronic transitions are suggested: The UV absorption with the pronounced peak at $\lambda = 260$ nm is observed with the complex as well as with the protonated ligand (not shown). This can be assigned to LC transitions of the aromatic groups, which are only slightly affected in energy and intensity by the oxidation state of the Mn ions. The band at 400 nm ($\varepsilon = 4600$ M^{-1}cm^{-1}) is presumably a CT transition from the bridging phenolate to Mn^{III} that has been observed between 320 and 400 nm with other phenoxo bridged $Mn_2^{II,III}$ and $Mn_2^{III,III}$ complexes.[9] The intensity of this bridging phenolate-Mn^{III} LMCT band has been reported to amount to as much as $\varepsilon = 2100$ M^{-1}cm^{-1} per phenoxo bond.[12] This value is in good agreement with the spectrum of **4** ($\varepsilon = 2300$ M^{-1}cm^{-1} per bridging phenoxo bond). The additional visible absorption might originate from LMCT transitions from other ligands, i.e. the nonbridging phenolate ligands or the pyridyl ligands, and also from a splitting of the metal d-orbitals due to the reduced symmetry of the complex. LF transitions of six-coordinated Mn^{III} complexes can occur in the visible

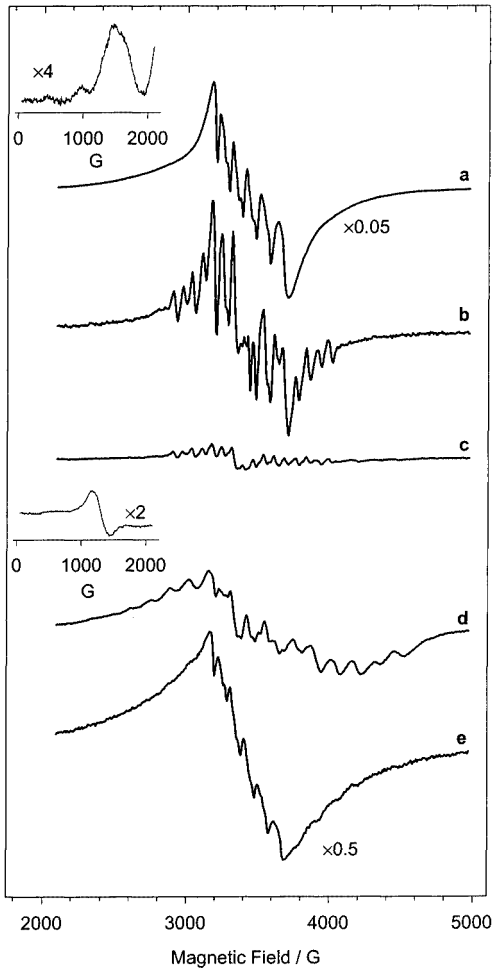

Figure 1. EPR spectra of **4** (1 mm, spectrum c) and its oxidation and reduction products in CH_3CN [0.1 M $N(n\text{-}C_4H_9)_4PF_6$] observed after electrolysis at −0.05 V (d), −0.50 V (e), 0.92 V (b) and 1.25 V (a). EPR parameters. *T*, 4 K; microwave frequency, 9.62 GHz; modulation amplitude, 10 G; microwave power, 3 mW (a, c, d), 0.3 mW (b, e). The spectra are normalized in amplitude (to the same microwave power, number of spectrometer scans, gain etc.) such that their size is approximately similar to facilitate comparison

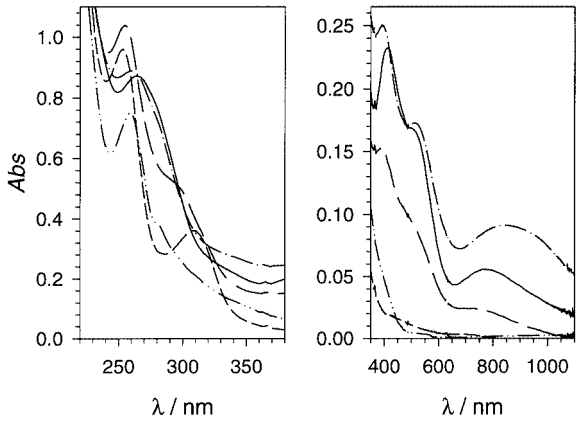

Figure 2. Electronic absorption spectrum of **4** ($5 \cdot 10^{-4}$ M, −) and spectra recorded after electrolysis at −0.05 V (− −), −0.60 V (---), 1.08 V (− · −), and 1.30 V (− · · −) in acetonitrile [0.1 M $N(n\text{-}C_4H_9)_4PF_6$]. $l = 1$ mm

region[13] but are of low intensities (typically $\varepsilon < 500$ $M^{-1}cm^{-1}$ [9a,14]).

IR Spectroscopy

IR spectra of ligand **3** and complex **4** (**4** as PF_6^- salt, see Supplementary Material) were recorded between 4000 and 400 cm^{-1}. Based on characteristic frequencies and comparison with the spectrum of **3,** the following assignments are suggested for the bands observed with **4** in agreement with the composition of the complex: 3082 cm^{-1}(w, ν C−H, aryl); 2954, 2907, 2868 cm^{-1} (s, ν C−H, alkyl); 1579cm^{-1} (s, ν_a C=O, carboxylate); 1605, 1571, 1478 cm^{-1}(m, ν C=C, aryl); 1430 cm^{-1}(m, ν_s C=O, carboxylate); 1384, 1361 cm^{-1} (w, δ C−H, alkyl); 844 cm^{-1}(s, ν_a P−F, PF_6^-); 761, 810 cm^{-1}(m, γ C−H, aryl); 558 cm^{-1} (m, δ P−F, PF_6^-). No assignment could be made for a number of weaker bands at 1247, 1171, 663, 617, 591 cm^{-1} of which the bands at 663 and 591 cm^{-1} were clearly absent in the spectrum of **3** and probably involve metal to ligand modes as ν Mn−O−Mn that were observed between 550 and 750 cm^{-1} with μ-oxo-bis(μ-carboxylato) $Mn^{III,III}$ complexes.[15]

The IR spectrum of **3** shows additional bands at about 3000 cm^{-1} (s, very broad, ν O−H with intramolecular H-bond), 1300 cm^{-1} (m, δ O−H) and 1111 cm^{-1} (m, ν C−O) that are diagnostic for the phenol functions of the ligand. These bands are not observed in the spectrum of **4** providing evidence that all phenol functions are deprotonated and ligated to the metal ions in **4** and that no or very little of the free ligand **3** is present in this preparation of **4**.

The value of Δν between the asymmetric and symmetric C=O stretch modes of the acetate ligands of **4** [$\Delta\nu = (\nu_a$ C=O) − (ν_s C=O) = 149 cm^{-1}], indicates that both acetate ligands are symmetrically bridging the two manganese(III) ions: For monodentate acetate ligands Δν is known to substantially exceed the free ionic value of $\Delta\nu = 164$ cm^{-1}, and for chelating acetate ligands Δν is usually smaller than the value observed with **4**.[16] Asymmetrically bridging carboxylates have been reported to show a greater Δν, similar to monodentate ligands.[17]

Electrochemistry

Cyclic and differential pulse voltammograms of **4** are shown in Figures 3 and 4 and the electrochemical data are summarized in Table 1. All potentials are reported vs. SCE (see Exp. Sect.). The cyclic voltammograms (see a in Figure 3) show two major quasi-reversible reduction waves labeled (1) and (2) and two almost merged oxidation waves labeled (3) and (4) that cannot be fully resolved even in differential pulse voltammetry (see b in Figure 3). A small reverse peak for the first oxidation is already observed with the low sweep rates (10 $mV{\cdot}s^{-1}$, not shown) but the minor reverse peak for the second oxidation only appears at higher sweep rates (≥ 500 $mV{\cdot}s^{-1}$). The one-electron nature of the reductions was confirmed coulometrically. Separate coulometric measurements on the individual oxidations are impeded by the small potential separation but the two oxidations correspond to two electrons in total.

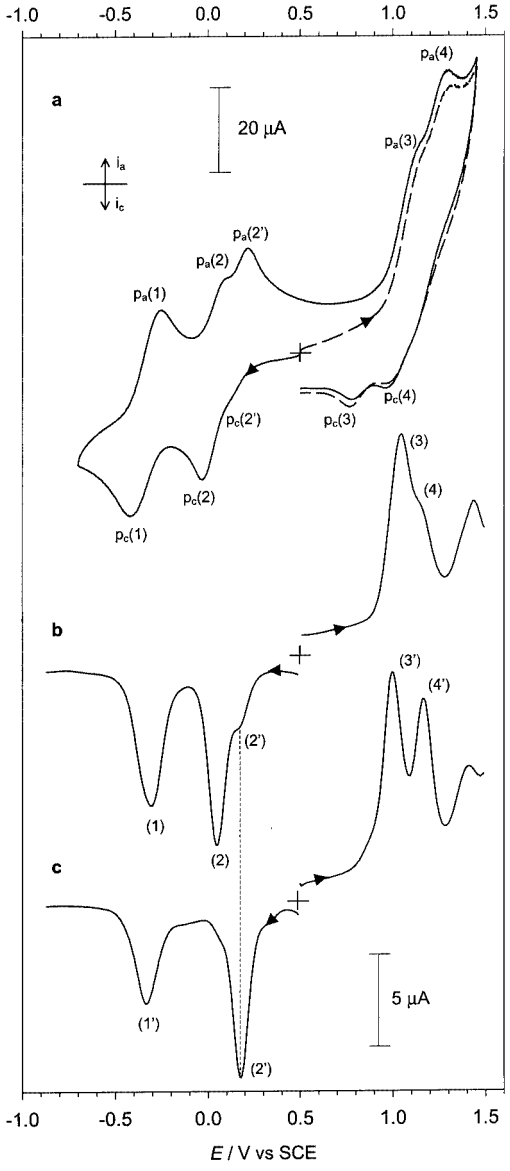

Figure 3. Cyclic voltammograms ($v = 500$ $mV{\cdot}s^{-1}$) (a) and differential pulse voltammogram (b) of **4** (1 mM) in acetonitrile (0.1 M $N(n\text{-}C_4H_9)_4PF_6$). Differential pulse voltammogram of a solution of **4** after exhaustive electrolysis at −0.10 V (c). Arrows indicate scanning direction

The minor quasi-reversible reduction wave (2′) in the cyclic voltammograms, that appears as a shoulder of the first reduction peak (2) in the differential pulse voltammogram (see b in Figure 3), is assigned to a different complex **4′** that is initially present, to a small extent, but is subsequently formed upon one-electron reduction of **4**. Evidence for this assignment comes from voltammograms observed immediately after exhaustive reduction of **4** at −0.10 V showing that the peak for the first reduction has shifted completely from $E(2)$ to $E(2')$ (compare b and c in Figure 3). A corresponding shift is observed for the re-oxidation peak when starting from the reduced complex. The conversion is quantitative (> 95%) as judged from the disappearance of the initial reduction peak (2) of **4**.

Table 1. Electrochemical data in acetonitrile

Complex	$E_{1/2}$ /V[a] (ΔE_p/mV)[b]			
	1	**2**	**3**	**4**
	$Mn_2^{II,III}/Mn_2^{II,II}$	$Mn_2^{III,III}/Mn_2^{II,III}$	$Mn_2^{III,IV}/Mn_2^{III,III}$	[c]
4[d]	−0.32 (140)	0.04 (130)	0.96 (360)	1.13 (340)
4′[d]	−0.34 (275)	0.17 (90)	0.95 (300)	1.13 (300)
$[Mn_2(bpmp)(\mu\text{-}OAc)_2]^{+}$ [e]	0.50 (70[f])	1.06 (120[f])	−[g]	−

[a] From cyclic voltammetry in CH_3CN, ±0.03 V. [b] v = 500 mV·s^{-1}. [c] The final oxidation product is a monomeric Mn^{II} or possibly Mn^{IV} complex. [d] As PF_6^- salt with 0.1 M $N(n\text{-}C_4H_9)_4PF_6$ as supporting electrolyte. [e] As ClO_4^- salt with 0.1 M $N(n\text{-}C_4H_9)_4ClO_4$ as supporting electrolyte. [f] v = 100 mV·s^{-1}. [g] No oxidation to the $Mn_2^{III,IV}$ state in CH_3CN.

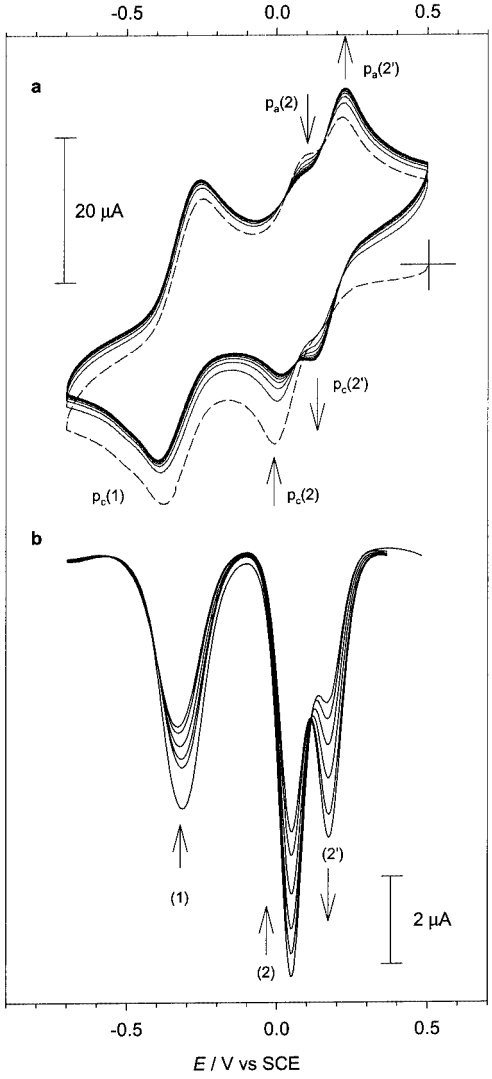

Figure 4. Voltammograms of **4** (1 mm) in acetonitrile [0.1 M $N(n\text{-}C_4H_9)_4PF_6$]. a) Cyclic voltammograms (v = 500 mV·s^{-1}). Scan 1 (- - -) and scans 2 to 10 (−). Arrows indicate the effect of increasing number of scans. b) Differential pulse voltammograms after increasing duration (0, 2, 5, 10, 20, 50 s) of pre-electrolysis at −0.10 V. Arrows indicate the effect of increasing pre-electrolysis time

A set of subsequent cyclic voltammograms of **4** (see a in Figure 4) shows how the reduction wave of **4′** grows with the expense of the reduction wave of **4**, as indicated by the arrows.

The same transformation was followed by differential pulse voltammograms (see b in Figure 4) recorded with increasing time of pre-electrolysis at −0.10 V, providing further evidence that the transformation to **4′** occurs in the one-electron reduced state of **4**.

The effect of this transformation on the potential for the first reduction is $\Delta E_{1/2}$ = 130 mV, while the effect on the second reduction (at −0.3 V) and the two oxidations (around 1 V) is comparatively small ($|\Delta E_{1/2}| \leq 0.05$ V) (see c in Figures 3, 4, Table 1).

The two reductions of both **4** and **4′** exhibit quasi-reversible CV waves (see a in Figure 4) but they are not reversible on the longer time-scale of the bulk electrolysis experiments (see below). For the oxidations of **4′** only small cathodic counter-peaks at $E_{pc}(3')$ = 0.80 V and $E_{pc}(4')$ = 0.98 V are observed on the reverse scan of the cyclic voltammograms (500 mV·s^{-1}, not shown) recorded after exhaustive electrolysis of **4** at −0.10 V. **4′** is unstable in its initial reduced state since well-defined voltammograms of **4′** were obtained only a few minutes after reduction of **4**. This will presumably impede isolation of **4′**. However, spectroscopic characterization of the reduced states of **4′** could be made immediately after reduction of **4**. (see below).

According to its EPR spectrum (see below) **4′** in its one-electron reduced state is a magnetically coupled $Mn_2^{II,III}$ dimer, the exact structure of which we cannot elucidate from our data. The loss of an acetate bridge from **4** as a charge compensating reaction due to reduction of the complex could explain the potential shift of the first reduction. However, with the loss of a negatively charged ligand a larger shift of *all* metal centered reduction and oxidation processes towards higher potentials would be expected. Therefore we suggest that the transformation of **4** into **4′** might instead represent a geometric re-arrangement of the reduced complex rather than loss or exchange of ligands.

Spectroscopic Characterization of the Reduced and Oxidized Products of 4

The products of the two reduction and the two-oxidation processes have been characterized by UV/Vis-spectroelectrochemistry and by EPR spectroscopy on samples prepared by electrolysis of **4** at appropriate potentials. Exhaustive electrolysis in the spectroelectrochemical experiments as well as for preparation of EPR samples occurs on

the time-scale of minutes, i.e. the species observed by these techniques upon *reduction* will be the reduction products of **4′**. The results of these experiments are discussed in the following paragraphs.

First Reduction

The first one-electron reduction of **4** can be assigned to a metal centered process [Equation (1)] resulting in a $Mn_2^{II,III}$ complex as evidenced by EPR spectroscopy.

$$[Mn_2^{III,III}L(\mu\text{-}OAc)_2]^+ + e^- \rightarrow [Mn_2^{II,III}L(\mu\text{-}OAc)_2] \qquad E_{1/2} = 0.04\ V \qquad (1)$$

The EPR spectrum of, **4** after exhaustive reduction at −0.05 V, displays a partially resolved multiline signal centered at $g \approx 2$ and a weak featureless signal at $g \approx 5.3$ (see d in Figure 1). The $g \approx 2$ multiline signal has a total line width of ca. 2300 G. The hyperfine lines are clearly visible but they are somewhat broadened. The relative amplitude of the $g \approx 2$ signal decreases while the $g \approx 5.3$ signal increases with increased temperature (not shown). This indicates that the $g \approx 2$ signal originates from a ground spin state while the $g \approx 5.3$ signal originates from an excited spin state. Similar overall behavior has been reported earlier for the EPR signals from $[Mn_2^{II,III}(bpmp)(\mu\text{-}OAc)_2]^{2+}$ [18], that is weakly antiferromagnetically coupled with a ground spin state $S = {}^1/_2$. In $[Mn_2^{II,III}(bpmp)(\mu\text{-}OAc)_2]^{2+}$ a featureless signal at $g \approx 5.4$ became detectable only above 7.5 K, while the multiline signal centered at $g \approx 2$ dominated at 4 K. In our case, however, the appearance of the relatively large $g \approx 5.3$ signal together with the $g \approx 2$ multiline signal already at 4 K, indicates that the excited spin state is lower in energy than in $[Mn_2^{II,III}(bpmp)(\mu\text{-}OAc)_2]^{2+}$. There are no parallel mode EPR signals of this sample (not shown), which is expected for an $S = {}^1/_2$ system. From EPR spectroscopy we therefore conclude that one electron reduction of **4** gives a weakly antiferromagnetically coupled $Mn_2^{II,III}$ species.

This assignment is in agreement with the spectrophotometrical changes observed during electrolysis at −0.05 V (Figure 2, − −): Upon the first reduction of **4** about half of the visible absorption disappears. Absorption at $\lambda >$ 400 nm has been assigned to the Mn^{III} subunit in the mixed valence $Mn_2^{II,III}$ state[9a] of the similar phenoxo bridged dinuclear manganese complex $[Mn_2(bpmp)(\mu\text{-}OAc)_2]^{2+}$. Therefore, the electronic spectrum corroborates the assignment of the first cathodic process to the formation of a $Mn^{II,III}$ complex. Several isosbestic points are observed in the course of the first reduction (not shown). This suggests that the structural changes of the reduced complex, that lead to the formation of **4′**, as indicated by voltammetry (see above), do not affect the absorption spectrum. Thus, they have a negligible effect on the phenolate to Mn^{III} CT transitions in the visible region and the ligand centered transitions in the UV part of the electronic spectrum.

Re-oxidation of the one-electron reduction product by bulk electrolysis was carried out at 0.60 V after exhaustive reduction at −0.05 V. According to coulometry only 55% of the material could be re-oxidized pointing to a limited stability of the one-electron reduction product. This is supported by the EPR spectrum of the re-oxidized sample (not shown) that can be assigned to uncoupled Mn^{II}, presumably from decomposition of the reduced complex, while the re-oxidized $Mn_2^{III,III}$ species can be expected to be EPR-silent. Note that the time-scale of bulk electrolysis is several minutes, which is much longer than that for the voltammetry experiments (Figures 3 and 4, and above).

Second Reduction

Further one-electron reduction of the $Mn_2^{II,III}$ complex at −0.50 V probably gives rise to both a dimeric $Mn_2^{II,II}$ and a monomeric Mn^{II} complex [Equation (2)].

$$[Mn_2^{II,III}L(\mu\text{-}OAc)_2] + e^- \rightarrow [Mn_2^{II,II}L(\mu\text{-}OAc)_2]^- + \text{monomeric } Mn^{II} \text{ species} \qquad E_{1/2} = -0.32\ V \qquad (2)$$

The EPR spectrum shows a broadened 6-line spectrum in the $g \approx 2$ region (see e in Figure 1) that can be assigned to a monomeric Mn^{II} species. Quantification of the EPR signal reveals that about 48% of the complex was found in the monomeric Mn^{II} form after the second reduction. Since all of the $Mn_2^{II,III}$ signals disappeared it is reasonable to assume that the residual 52% of the complex was kept in the $Mn_2^{II,II}$ state after the second reduction.

This is supported by the observation of an EPR spectrum with parallel mode EPR (Figure 5). This featureless spectrum covers the spectral range from 0−3000 G and indicates the presence of a species with integral spin. Monomeric Mn^{II} species with $S = {}^1/_2$ are not expected to give rise to spectra of this kind. To the best of our knowledge there are no literature reports of parallel mode EPR studies for $Mn^{II,II}$ compounds but spectra of this kind cannot be excluded for antiferromagnetically coupled dimers.

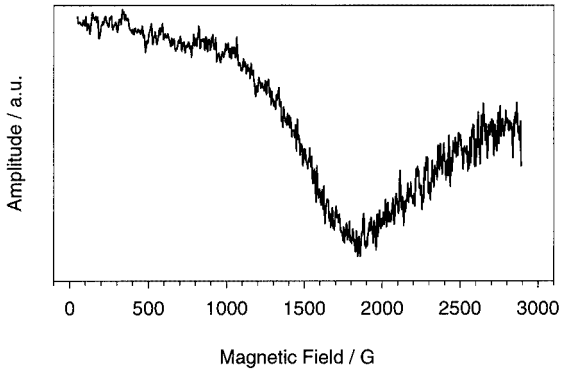

Figure 5. EPR spectrum recorded in parallel mode after bulk electrolysis of **4** at −0.50 V. The spectrum is recorded on the same sample as in Figure 1e. $T = 4$ K; microwave power 16 mW; modulation amplitude 10 G; microwave frequency 9.47 GHz

Reductive degradation of the ligand is unlikely at this potential and presumably a $Mn_2^{II,II}$ complex is formed initially that undergoes some subsequent dissociation reaction giving the monomeric Mn^{II} species observed by EPR.

The assignment of the second reduction to the reduction of Mn^{III} centers to Mn^{II} is in agreement with the spectrophotometric changes: Most of the residual visible absorption of the $Mn_2^{II,III}$ complex disappears upon the second one-electron reduction (Figure 2, ---) as expected from the usually low intensity of MLCT transitions of Mn^{II}. Similar spectral changes have been reported for the reduction of $[Mn_2^{II,III}(bpmp)(\mu\text{-}OAc)_2]^{2+}$ to the $Mn_2^{II,II}$ state.[9a]

First Oxidation

4 can be oxidized in two irreversible one-electron steps that occur very close in potential (Figure 3), making the study of the individual oxidation products of the respective oxidation process more complicated. Still the first oxidation can be assigned to a metal centered process resulting in a $Mn_2^{III,IV}$ dimer [Equation (3)] detected by EPR spectroscopy.

$$[Mn_2^{III,III}L(\mu\text{-}OAc)_2]^{+} \rightarrow [Mn_2^{III,IV}L(\mu\text{-}OAc)_2]^{2+} + e^{-} \qquad E_{1/2} = 0.96\ V \qquad (3)$$

The EPR spectrum in Figure 1 (see b) was observed after partial oxidation of **4** at 0.92 V, i.e. at a potential 40 mV *below* $E_{1/2}$ for the first oxidation. At this potential only a minor fraction of the complex can be expected to be oxidized but further oxidation due to the nearby second anodic process is avoided. The resulting EPR spectrum displays a well-resolved multiline signal (see b in Figure 1). This multiline signal consists of 18−19 lines centered at $g \approx 2$, with an overall line width of 1115 G, and an average hyperfine splitting of ca. 73 G. The spectrum is thus much narrower than that for the one-electron reduced $Mn_2^{II,III}$ product of **4** (see above). A narrow multiline EPR signal of this character (see b in Figure 1) is typical for a $Mn_2^{III,IV}$ dimer that is strongly antiferromagnetically coupled with a resulting spin of $S = {}^1/_2$.[19] Integration of the signal and comparison with a $Mn_2^{III,IV}$ standard (see Exp. Sect.) shows that this multiline spectrum corresponds to about 0.2 mM of $Mn_2^{III,IV}$ after oxidation of a 1 mM solution of **4**. This is similar to the 0.3 charge equivalents determined coulometrically for oxidation of the EPR sample demonstrating that oxidation at 0.92 V is predominantly a metal centered reaction resulting in $Mn_2^{III,IV}$. The multiline signal from the $Mn_2^{III,IV}$ disappeared almost completely (not shown) after re-reduction at 0.50 V. However, for this reduction only 0.04 charge equivalents were consumed, pointing to limited stability of the $Mn_2^{III,IV}$ state. This might also explain that the concentration of $Mn_2^{III,IV}$ after bulk electrolysis is somewhat lower than expected from coulometry.

At higher potentials, such as 1.05 V, electrolysis results in a mixture of oxidation products as the EPR spectra (not shown) are a superposition of a multiline signal from $Mn_2^{III,IV}$ as described above and a 6-line signal that is probably due to monomeric Mn^{II} (see below). Upon re-reduction of this sample at 0.50 V, the multi-line spectrum disappeared while the 6-line spectrum remained, supporting the assignment of the spectra to a $Mn_2^{III,IV}$ complex and Mn^{II}, respectively. Since no 6-line signal was observed upon oxidation at lower potentials, such as 0.92 V (see above), the species giving rise to this signal is presumably a product of the second anodic process.

The spectrophotometrical changes observed upon oxidation of **4** at 1.05 V corroborate the conclusions drawn from the EPR results. The increased absorption in the region 500−1100 nm upon oxidation at 1.08 V (Figure 2, − · −) can be assigned to the $Mn_2^{III,IV}$ complex detected by EPR spectroscopy. Absorption bands observed between 500 and 935 nm have been assigned to phenolate to Mn^{IV} LMCT transitions in Mn^{IV} monomeric complexes[20] as well as $Mn_2^{III,IV}$ and $Mn_2^{IV,IV}$ dimers[21] and bands at $\lambda > 700$ nm have been assigned to intervalence transitions in mixed-valence μ-oxo $Mn_2^{III,IV}$ complexes.[22] Isosbestic points were observed at the outset ($t < 300$ s) of the spectroelectrochemical experiment (not shown). Throughout the course of electrolysis, however, the isosbestic points were not maintained either due to instability of the $Mn_2^{III,IV}$ species or parallel formation of oxidation products from the second oxidation process. This is consistent with the EPR spectroscopic results that show a 6-line spectrum besides the spectrum of the Mn_2III,IV complex after oxidation at this potential (1.05 V).

Second Oxidation

Oxidation at 1.25 V [Equation (4)] gives rise to EPR spectra dominated by a 6-line signal centered at $g \approx 2$ with a hyperfine coupling of ca. 95 G (see a in Figure 1).

$$[Mn_2^{III,IV}L(\mu\text{-}OAc)_2]^{2+} \rightarrow \text{oxidation products} + e^{-} \qquad E_{1/2} = 1.13\ V \qquad (4)$$

The EPR spectrum of the product is identical to the 6-line signal for the sample oxidized at 1.05 V (not shown, see above). A detailed inspection of the lower field region reveals the presence of a very weak signal at g ≈ 4 (inset in Figure 1). The 6-line spectral feature (see a in Figure 1) is very similar to a typical spectrum from monomeric Mn^{II} and we assign this spectrum to Mn^{II}. This assignment is also based on the spectroelectrochemical studies where the complete disappearance of visible and near infrared absorption upon the second oxidation (Figure 2, − · · −) suggests that the second oxidation process generates monomeric Mn^{II} rather than Mn^{IV}, since Mn^{IV} phenolate complexes are known to show intense LMCT transitions in the visible region.[20] Thus, it seems that **4** is degraded during the second oxidation step probably involving ligand oxidation at the relatively high potential that is employed. In the course of the second oxidation isosbestic points are absent (not shown). This is in agreement with a more complicated reaction scheme that possibly involves phenolate ligand oxidation[23] finally resulting in the release of monomeric Mn^{II}.

The very weak EPR signal at $g \approx 4$ might however originate from a trace of Mn^{IV} remaining after the oxidation although the fraction is too small to give a measurable absorption in UV/Vis spectroelectrochemistry (Figure 2). Monomeric Mn^{IV} has been reported to give rise to a 6-line signal around $g \approx 2$, quite similar in shape to the signal

from Mn^{II}, in addition to the weak $g \approx 4$ signal.[20e] It is thus difficult to distinguish Mn^{IV} from Mn^{II} in the $g \approx 2$ region while the $g \approx 4$ region probably is more indicative.

The possible generation of a Mn^{IV} containing state at a high potential in **4** is interesting, although one has to use techniques more rapid than bulk electrolysis to trap and detect it and possibly utilize its oxidative power.

Conclusions

The negative charge of the three phenolate groups in **4** results in a considerable stabilization of higher oxidation states of the Mn ions compared to the case of $[Mn_2(bpmp)(\mu\text{-}OAc)_2]^+$ [9a] that has only one bridging phenoxo group of the bpmp ligand. The stabilization is reflected in the electrochemical potentials summarized in Table 1. The potentials for the $Mn_2^{II,III}/Mn_2^{II,II}$, and $Mn_2^{III,III}/Mn_2^{II,III}$ couples of **4** are lowered by 0.8 and 1.0 V compared with $[Mn_2(bpmp)(\mu\text{-}OAc)_2]^+$, and a third metal centered process attributable to the $Mn_2^{III,IV}/Mn_2^{III,III}$ couple is observed with **4** before oxidative degradation of the complex occurs. With regard to our interest in systems as functional mimics of the water oxidizing complex in Photosystem II, it is worth pointing out that due to the stabilization of high valent Mn states all four of the reported oxidation steps of **4** could be driven with photogenerated $Ru(bpy)_3^{3+}$ ($E_{1/2}$ = 1.32 V). However, accumulation and subsequent use of oxidative equivalents would require a rapid redox cycling in order to outcompete degradation of the less stable states of **4**.

Experimental Section

Materials: Triethylamine and ammonium hexafluorophosphate were purchased from Aldrich and used as received. Silica gel 60 (230−400 mesh) from Merck, Darmstadt, Germany and Aluminum oxide from Aldrich. All solvents were dried by standard methods. 2-aminomethylpyridine was purchased from Lancaster. 3,5-di-*tert*-butyl-2-hydroxybenzaldehyde was purchased from Aldrich and used without further purification.

General Methods: NMR spectra were measured either on Bruker-400 MHz spectrometer for 1D or on a Bruker-500 MHz spectrometer for 2D. The positions of the signals are reported on δ scale in ppm units. The splitting of the signal is described as singlets (s), doublets (d), triplets (t), quadruplets (q), doublets of doublets (dd), or multiplets (m).

The electrospray ionization mass spectrometry (ESI-MS) experiments were performed on a ZacSpec mass spectrometer (VG Analytical, Fisons Instrument). Electrospray conditions were: Needle potential, 3 kV; acceleration voltage, 4 kV; bath and nebulizing gas, nitrogen. The liquid flow was 75 μL per min from a syringe pump (Phoenix 20, Carlo−Erba, Fisons instrument). Solvent, CH_3CN. Accurate mass measurements were obtained by the use of polyethylene glycol (PEG) as an internal standard.

Thin-layer chromatography (TLC) was performed using silica gel (Kieselgel F_{254}) adsorbent.

Column chromatography was performed using silica gel (Kieselgel 60, 0.040−0.063 mm).

Synthesis of *N*-(3,5-Di-*tert*-butyl-2-hydroxy)-*N*-(2-pyridylmethyl)-amine (1): 3,5-di-*tert*-butyl-2-hydroxybenzaldehyde (1.48 g, 6.32 mmol) and picolylamine (0.68 g, 6.32 mmol) were dissolved in MeOH (30 mL) and stirred for 4 hours at 50° C. After cooling to room temperature, $NaBH_4$ (0.34 g, 9 mmol) was added to the solution in small amounts and the solution was stirred for another 4 hours at room temperature. After evaporating the solvent to dryness, the residue was dissolved in CH_2Cl_2 and washed with an aqueous solution of NH_4Cl and dried with Na_2SO_4. 1.20 g (61%) of product was obtained after purification by flash chromatography on silica gel eluting with CH_2Cl_2. ^1H NMR ($CDCl_3$, 400 MHz): δ = 8.58 (d, H-Py); 7.66 (t, H-Py); 7.23 (m, 2 H-Py); 6.84 (d, 2 H-Ph); 3.98 (s, N-CH_2-Py); 3.94 (s, N-CH_2-Ph); 1.43 (s, *tert*-Butyl); 1.28 (s, *tert*-Butyl) ppm.

Synthesis of 2,6-Bis(chloromethyl)-4-methylphenol (2):[24] A solution of 2,6-bis(hydroxymethyl)-4-methylphenol (2.5 g,,15 mmol) in dichloromethane (12.5 mL) was added to a solution of thionyl chloride (7.0 g,60 mmol) in dichloromethane (25 mL). After stirring for 24 hours the mixture was poured over ice (25 mL) and adjusted to pH = 6 with aqueous NaOH. The aqueous solution was extracted with three 25 mL portions of dichloromethane, washed with brine and dried with anhydrous Na_2SO_4. The solution was evaporated to dryness at reduced pressure yielding a pale-yellow solid. By recrystallization from hexane 1.85 g (yield: 60%) of the product was obtained and stored in a freezer. mp: 80° C. ^1H NMR ($CDCl_3$, 400 MHz, ppm): 7.09 (s, 2 H, Ar-H), 4.66 (s, 4 H, Ar-CH_2-Cl), 2.28 (s, 3 H, Ar-CH_3).

Synthesis of 2,6-Bis{[(3,5-di-*tert*-butylbenzyl-2-hydroxy)(2-pyridylmethyl)amino]methyl}-4-methylphenol (3)[25] A solution of (3,5-di-*tert*-butylbenzyl-2-hydroxy)(2-pyridylmethyl)amine (2.1 g, 6.4 mmol) and triethylamine (1.3 g, 13 mmol) in THF (20 mL) was added dropwise to 10 mL of a stirred solution of 2,6-bis(chloromethyl)-4-methylphenol (0.6 g, 3.2 mmol) in THF at 0° C under nitrogen atmosphere. The reaction mixture was stirred for 12 hours at room temperature. Then the solution was filtered to remove the TEA salts, the filtrate was evaporated to dryness and the residue was dissolved in CH_2Cl_2 (80 mL) and washed with brine. The organic phase was dried with anhydrous Na_2SO_4. The product was purified by flash chromatography on silica gel, eluting with CH_2Cl_2. 1.32 g of product was obtained, yield: 52%. ^1H NMR ($CDCl_3$, 400 MHz, ppm): 8.60 (d, H-Py); 7.65 (t, H-Py); 7.31 (d, H-Py); 7.22 (t, H-Ph); 7.16 (d, H-Ph); 6.93 (s, H-Ph); 6.83 (d, H-Ph); 3.83 (s, N−CH_2-Py); 3.78 (s, N−CH_2-Ph); 3.76 (s, N−CH_2-Ph); 2.22 (s, CH_3-Ph); 1.32 (s, *tert*-butyl-Ph); 1.25 (s, *tert*-butyl-Ph).

The Complex of $Mn(OAc)_3(H_2O)_2$ with 2,6-Bis{[(3,5-di-*tert*-butylbenzyl-2-hydroxy)(2-pyridylmethyl)amino]methyl}-4-methylphenol (4):[9a] $Mn(OAc)_3(H_2O)_2$ (95.0 mg, 0.35 mmol) was added to 2,6-bis{[(3,5-di-*tert*-butylbenzyl-2-hydroxy)(2-pyridylmethyl)amino]-methyl}-4-methylphenol (**3**) (135.0 mg, 0.17 mmol) in 85% ethanol (3 mL). The mixture was heated at 50 °C for 30 min and cooled to room temperature. NH_4PF_6 (81 mg, 0.49 mmol) in 85% ethanol (1 mL) was added to the red-brown solution whilst stirring, and the solution was stored in a freezer overnight. The solid was filtered off and washed with 85% ethanol (1.5 mL) at 0° C, H_2O (2 mL) and 99% ethanol (1.5 mL). After drying under vacuum, 151 mg of solid product was obtained. Yield: 86%. ESI-MS: (*m*/*z*): 1009.4 [M − PF_6]$^+$ (calcd. for $C_{55}H_{71}N_4O_7Mn_2$: 1010.06), 2163.8 [2 M − PF_6]$^+$ (calcd. for $C_{110}H_{142}N_8O_{14}F_6PMn_4$: 2165.08); $C_{55}H_{71}F_6Mn_2N_4O_7P$ (1155.02): calcd. C 57.19, H 6.20, N 4.85, Mn 9.51; found C 57.16, H 6.26, N 4.82, Mn 9.44.

Electrochemistry: Cyclic voltammetry, differential pulse voltammetry, and controlled potential electrolysis were performed with an Autolab potentiostat and a GPES electrochemical interface in a 3-electrode cell with the counter electrode separated from the bulk by a fritted disk. The working electrode was a glassy carbon disc (diameter 3 mm) for voltammetry or a platinum grid cylinder (15 mm × 15 mm diameter) for bulk electrolysis, respectively. The reference electrode was a nonaqueous Ag/Ag^+ electrode (10 mM $AgNO_3$ in acetonitrile) of double-junction design. The reference electrode has a potential of −0.08 V vs. the ferrocene/ferrocenium couple in acetonitrile as an external standard. All potentials reported here are vs. the saturated calomel electrode (SCE) and have been converted by adding 0.30 V to the potentials measured vs. the Ag/Ag^+ electrode according to $E_{1/2} = 0.38$ V vs. SCE for the ferrocene/ferrocenium couple.[26]

Electrolyte solutions were prepared from dry acetonitrile (Merck, spectroscopy grade, dried with MS 3 Å) with 0.1 M tetrabutylammonium hexafluorophosphate (Fluka, electrochemical grade, dried at 373 K) as supporting electrolyte. The glassware used was oven dried, assembled and flushed with argon while hot. Before all measurements, the solutions were deoxygenated by bubbling solvent saturated argon through the stirred solutions for 10 minutes. Whilst measuring the samples were kept under an argon atmosphere.

The electrochemical preparation of EPR samples was performed by bulk electrolysis of 1 mm (3 mL) solutions at controlled potentials. The electrolysis was followed by amperometry and coulometry. After electrolysis, samples of 250 μL were taken with an argon filled syringe via a septum from the electrolysis vessel and transferred to argon flushed EPR tubes. The samples were immediately frozen and kept in liquid nitrogen.

UV/Vis Spectroelectrochemistry: Spectroelectrochemical measurements were made in an OTTLE-type quartz cell with an optical path length of 1 mm. A platinum grid of size 10 × 30 mm^2 and 400 meshes per cm^2 was used as working electrode. The counter and reference electrodes were of the same type as described for electrochemistry. Solvent saturated argon was bubbled through samples for 15 min, and they were then transferred to the argon flushed cell with an argon stream. The spectra were recorded on an UV/Vis diode array spectrophotometer (Hewlett Packard 8435).

IR Spectroscopy: IR spectra were recorded on a FT-IR spectrometer (Bruker IFS 66v/S) with the sample as a KBr pellet.

EPR Spectroscopy: All EPR spectra were recorded on a Bruker E580-ELEXSYS spectrometer equipped with an Oxford 900 liquid helium cryostat and an ITC 503 temperature controller. An ER4116DM dual mode X-band resonator of rectangular type (TE_{102} for perpendicular and TE_{012} for parallel mode) was used for all measurements. Data analysis was carried out with either the X-Epr or X-Winpro software packages.

Quantification of **4** in different oxidation states was carried out by double integration of the perpendicular EPR mode signal studied within the selected spectral region. The signal intensity was then converted into spin concentration by comparison with the signal intensity in a standard sample in the same oxidation state with known concentration. All EPR spectra used for the evaluation of the different concentrations were recorded using nonsaturating microwave power.

The amount of $Mn_2^{II,III}$ found in the preparation of **4** was obtained by comparison with the signal in the $g = 2$ region recorded after exhaustive one electron reduction of **4** to the $Mn_2^{II,III}$ state. The reduction was monitored coulometrically providing the exact concentration of $Mn_2^{II,III}$ after electrolysis.

$[Mn_2^{III,IV}(\mu\text{-}O)_2(bpy)_4]^{3+}$ was utilized as the standard for quantification of the $Mn_2^{III,IV}$ complex formed after one-electron oxidation of **4**. The precise concentration of the $[Mn_2^{III,IV}(\mu\text{-}O)_2(bpy)_4]^{3+}$ standard was determined spectrophotometrically at 684 nm.[27]

Mn^{II} acetate (purity > 99.9%) in 10% water/90% acetonitrile was used as standard for quantification of monomeric Mn^{II} species formed, e.g. after two-electron reduction. Mn^{II} acetate was used as purchased.

Magnetic Susceptibility Measurements: Magnetic susceptibility measurements were performed on an MPMS5 magnetometer (Quantum Design Inc.) over a temperature range of 2−300 K and at a magnetic field of 1.0 T. A palladium reference (Quantum Design Inc.) was used for callibration at 298 K. Data were corrected for diamagnetism and the χT vs. T plot was fitted according to the procedure described in ref.[28]

Acknowledgments

Eric Rivière (Université Paris-Sud, Orsay) is gratefully acknowledged for performing and analyzing the magnetic susceptibility measurements. This work was supported by the Knut and Alice Wallenberg Foundation, the Swedish National Energy Administration, the Swedish Research Council, and DESS.

[1] [1a] Thematic issue: *Biochim. Biophys. Acta* **2001**, *1503*, 1− 259. [1b] R. D. Britt, in: *Oxygenic Photosynthesis: The Light Reactions* (Ed.: D. R. Ort, C. F. Yocum), Kluwer Academic Publishers, Dordrecht, **1996**, pp 137−164. [1c] W. Ruttinger, G. C. Dismukes, *Chem. Rev.* **1997**, *97*, 1−24.

[2] [2a] L. Sun, L. Hammarström, B. Åkermark, S. Styring, *Chem. Soc. Rev.* **2001**, *30*, 36−49. [2b] M. Yagi, M. Kaneko, *Chem. Rev.* **2001**, *101*, 21−35. [2c] See ref.[1c]

[3] bpmp = 2,6-bis[bis(2-pyridylmethyl)amino]methyl-4-methylphenol.

[4] [4a] L. Sun, M. K. Raymond, A. Magnuson, D. LeGourriérec, M. Tamm, M. Abrahamsson, P. Huang-Kenéz, J. Mårtensson, G. Stenhagen, L. Hammarström, S. Styring, B. Åkermark, *J. Inorg. Biochem.* **2000**, *78*, 15−22. [4b] P. Huang-Kenéz, A. Magnuson, R. Lomoth, M. Abrahamsson, M. Tamm, L. Sun, B. van Rotterdam, J. Park, L. Hammarström, B. Åkermark, S. Styring, *J. Inorg. Biochem.* **2002**, *91*, 159−172.

[5] [5a] J. H. Robblee, R. M. Cinco, V. K. Yachandra, *Biochim. Biophys. Acta* **2001**, *1503*, 7−23 and references therein. [5b] D. Kuzek, R. J. Pace, *Biochim. Biophys. Acta* **2001**, *1503*, 123−137. [5c] G. Renger, *Biochim. Biophys. Acta* **2001**, *1503*, 210−228. [5d] V. K. Yachandra, K. Sauer, M. P. Klein, *Chem. Rev.* **1996**, *96*, 2927−2950.

[6] P. E. M. Siegbahn, R. H. Crabtree, *J. Am. Chem. Soc.* **1999**, *121*, 117−127.

[7] [7a] J. Limburg, J. S. Vrettos, L. M. Liable-Sands, A. L. Rheingold, R. H. Crabtree, G. W. Brudvig, *Science* **1999**, *283*, 1542−1527. [7b] J. Limburg, J. S. Vrettos, H. Chen, J. C. de Paula, R. H. Crabtree, G. W. Brudvig, *J. Am. Chem. Soc.* **2001**, *123*, 423−430. [7c] J. S. Vrettos, J. Limburg, G. W. Brudwig, *Biochim. Biophys. Acta* **2001**, *1503*, 229−245.

[8] A. Neves, M. A. de Brito, I. Vencato, V. Drago, K. Griesar, W. Haase, *Inorg. Chem.* **1996**, *35*, 2360−2368.

[9] [9a] H. Diril, H.-R. Chang, M. J. Nilges, X. Zhang, J. A. Potenza, H. J. Schugar, S. S. Isied, D. N. Hendrickson, *J. Am. Chem. Soc.* **1989**, *111*, 5102−5114. [9b] M. Suzuki, M. Miku-

riya, S. Murata, A. Uehara, H. Oshio, S. Kida, K. Saito, *Bul. Chem. Soc. Jpn.* **1987**, *60*, 4305−4312.
[10] See ref.[14b]
[11] [11a] K. A. Campbell, PhD thesis, University of California, Davis, **1999**. [11b] T. Yamauchi, H. Mino, T. Matsukawa, A. Kawamori, T. Ono, *Biochemistry* **1997**, *36*, 7520−7526.
[12] J. B. Vincent, K. Folting, J. C. Huffman, G. Christou, *Inorg. Chem.* **1986**, *25*, 996−999.
[13] E. König, S. Kremer, *Ligand Field Energy Diagrams*, Plenum Press, New York, **1977**, 175−200.
[14] K. Yamaguchi, D. T. Sawyer, *Inorg. Chem.* **1985**, *24*, 971−976.
[15] J. E. Sheats, R. S. Czernuszewicz, G. C. Dismukes, A. L. Rheingold, V. Petrouleas, J. Stubbe, W. H. Armstrong, R. H. Beer, S. J. Lippard, *J. Am. Chem. Soc.* **1987**, *109*, 1435−1444.
[16] G. B. Deacon, R. J. Phillips, *Coord. Chem. Rev.* **1980**, *23*, 227−250.
[17] M. Suzuki, M. Mikuriya, S. Murata, A. Uehara, H. Oshio, S. Kida, K. Saito, *Bull. Chem. Soc. Jpn.* **1987**, *60*, 4305−4312.
[18] [18a] H. Diril, H.-R. Chang, X. Zhang, S. K. Larsen, J. A. Potenza, C. G. Pierpont, H. J. Schugar, S. S. Isied, D. N. Hendrickson, *J. Am. Chem. Soc.* **1987**, *109*, 6207−6208. [18b] H-R. Chang, S. K. Larsen, P. W. Boyd, C. G. Pierpont, D. N. Hendrickson, *J. Am. Chem. Soc.* **1988**, *110*, 4565−4576.
[19] [19a] M. Zheng, S. V. Khangulov, G. C. Dismukes, V. V. Barynin, *Inorg. Chem.* **1994**, *33*, 382−387. [19b] P. J. Pessiki, S. V. Khangulov, D. M. Ho, G. C. Dismukes, *J. Am. Chem. Soc.* **1994**, *116*, 891−897.
[20] [20a] H. Okawa, M. Nakamura, S. Kida, *Bull. Chem. Soc. Jpn.* **1982**, *55*, 466−470. [20b] D. P. Kessisoglou, X. Li, W. M. Butler, V. L. Pecoraro, *Inorg. Chem.* **1987**, *26*, 2487−2492. [20c] U. Auerbach, T. Weyhermüller, K. Wieghardt, B. Nuber, E. Bill, C. Butzlaff, A. X. Trautwein, *Inorg. Chem.* **1993**, *32*, 508−519. [20d] A. Neves, S. M. D. Erthal, I. Vencato, A. S. Ceccato, Y. P. Mascarenhas, O. R. Nascimento, M. Hörner, A. A. Batista, *Inorg. Chem.* **1992**, *31*, 4749−4755. [20e] S. K. Chandra, A. Chakravorty, *Inorg. Chem.* **1992**, *31*, 760−765. [20f] S. K. Chandra, P. Basu, D. Ray, S. Pal, A. Chakravorty, *Inorg. Chem.* **1990**, *29*, 2423−2428.
[21] [21a] O. Horner, E. Anxolabéhère-Mallart, M.-F. Charlot, L. Tchertanov, J. Guilhem, T. A. Mattioli, A. Boussac, J.-J. Girerd, *Inorg. Chem.* **1999**, *38*, 1222−1232. [21b] M. J. Baldwin, T. L. Stemmler, P. J. Riggs-Gelasco, M. L. Kirk, J. E. Penner-Hahn, V. L. Pecoraro, *J. Am. Chem. Soc.* **1994**, *116*, 11349−11356.
[22] P. A. Goodson, J. Glerup, D. J. Hodgson, K. Michelsen, E. Pedersen, *Inorg. Chem.* **1990**, *29*, 503−508.
[23] Mn(Ph−O$^{\cdot}$) states of monomeric complexes have been reported (ref.[23]) and generation of a $Mn_2^{III,IV}$(Ph−O$^{\cdot}$) species has also been observed in a dimer with nonbridging phenolates (ref.[21a]). In our case no Ph−O$^{\cdot}$ species was sufficiently stable to be observed on the time-scale of electrolysis. [23a] J. Müller, A. Kikuchi, E. Bill, T. Weyhermüller, P. Hildebrandt, L. Ould-Moussa, K. Wieghardt, *Inorg. Chim. Acta* **2000**, *297*, 265−277. [23b] H. Schmitt, R. Lomoth, A. Magnuson-Styring, J. Park, J. Fryxelius, M. Kritikos, J. M Årtensson, L. Hammarström, L. Sun, B. Åkermark, *Chem. Eur. J.* **2002**, *8*, 3757−3768.
[24] [24a] A. S. Borovik, V. Papaefthymiou, L. F. Taylor, O. P. Anderson, L. Que Jr., *J. Am. Chem. Soc.* **1989**, *111*, 6183−6195. [24b] H. P. Berends, D. W. Stephan, *Inorg. Chem.* **1987**, *26*, 749−754.
[25] K. J. Oberhausen, J. F. Richardson, R. M. Buchanan, J. K. McCusker, D. N. Hendrickson, J. M. Latour, *Inorg. Chem.* **1991**, *30*, 1357−1365.
[26] V. V. Pavlishchuk, A. W. Addison, *Inorg. Chim. Acta* **2000**, *298*, 97−102.
[27] R. Manchanda, G. W. Brudvig, R. H. Crabtree, *New J. Chem.* **1994**, *18*, 561−568.
[28] S. Poussereau, G. Blondin, G. Chottard, J. Guilhelm, L. Tchertanov, E. Rivière, J.-J. Girerd, *Eur. J. Inorg. Chem.* **2001**, 1057−1062.

Received February 6, 2002
[I02060]